Thermal stress in a ceramic brick air preheater
by Rodney Carl Harris

A thesis submitted in partial fulfillment of the requirements for the degree of MASTER OF SCIENCE in Mechanical Engineering
Montana State University

Abstract:
Thermal stresses were calculated for an experimental magnetohydrodynamic cored ceramic brick regenerative air preheater. The finite element method was employed for determining both temperature and stress distributions for individual ceramic core bricks at typical cyclic equilibrium operating conditions. Maximum stress values and their locations in the hexagonal core bricks were calculated and compared with values predicted by an earlier, more approximate method as well as with failure modes in an actual preheater. The maximum stresses were found to be circumferential; that is, acting perpendicularly to the direction of the gas flow passages.

STATEMENT OF PERMISSION TO COPY

In presenting this thesis in partial fulfillment of the requirements for an advanced degree at Montana State University, I agree that the Library shall make it freely available for inspection. I further agree that permission for extensive copying of this thesis for scholarly purposes may be granted by my major professor, or, in his absence, by the Director of Libraries. It is understood that any copying or publication of this thesis for financial gain shall not be allowed without my written permission.

Signature Rodney Carl Harris

Date Sept 19 1978

THERMAL STRESS IN A CERAMIC BRICK AIR PREHEATER

by

RODNEY CARL HARRIS

A thesis submitted in partial fulfillment
of the requirements for the degree

of

MASTER OF SCIENCE

in

Mechanical Engineering

Approved:

Thomas C. Reihman
Chairperson, Graduate Committee

Dennis O. Blackketter
Head, Major Department

Henry L. Parsons
Graduate Dean

MONTANA STATE UNIVERSITY
Bozeman, Montana

September, 1978

ACKNOWLEDGEMENTS

The author would like to acknowledge Dr. T. C. Reihman, Dr. R. L. Mussulman, Dr. H. W. Townes, Dr. R. C. Oakberg, and Dr. R. L. Brown for their help and guidance in researching this thesis. The author would also like to thank his parents and Arlene Van Woert for encouragement and Charlene Edwards for the typing.

TABLE OF CONTENTS

LIST OF TABLES

LIST OF FIGURES

NOMENCLATURE

Symbol	Description
a	flow hole radius
b	equivalent flow hole outer radius
D	flow hole diameter
E	ceramic Young's Modulus
EOB	end of blowdown
EOR	end of reheat
F_{i-j}	shape factor from surface i to surface j
f	Darcy-Weisbach friction factor
f_o	Darcy-Weisbach friction factor for smooth pipe
f_r	Darcy-Weisbach friction factor for rough pipe
g	acceleration of gravity
Gr_δ	perimeter gap Grashof number
h_c	brick perimeter convective coefficient
h_f	flow hole convective coefficient
h_r	brick perimeter equivalent radiative coefficient
h_T	brick perimeter total convective coefficient
k_c	ceramic thermal conductivity
k_g	flow hole gas thermal conductivity
k_{g_p}	perimeter gap gas thermal conductivity
k_s	flow hole equivalent sand grain roughness
N	number of radiative surfaces

Symbol	Description
Nu	flow hole local Nusselt number
Nu_{δ}	perimeter gap Nusselt number
Pr	flow hole local Prandtl number
Q	heat flux at flow hole surface (Upshaw)
q_f	heat flux at flow hole surface
q_i	radiant heat flux at surface i
q_w	heat flux at brick perimeter
Re	flow hole local Reynolds number
R_i	radiosity of surface i
s	flow hole spacing
T_c	ceramic temperature at flow hole surface
T_g	flow hole gas temperature
T_{gb}	blowdown gas temperature
T_i	temperature of surface i
T_1	brick perimeter ceramic temperature
T_2	containment tube temperature
Z	distance from flow hole entrance
α	ceramic thermal expansion coefficient
β	volume coefficient of expansion of an ideal gas
σ	Stephan-Boltzmann constant
σ_{max}	maximum tantential stress at the flow hole surface
μ	perimeter gap gas viscosity

Symbol	Description
ε_i	emissivity of surface i
ρ	reflectivity of surface i
ν	ceramic Poisson's ratio

ABSTRACT

Thermal stresses were calculated for an experimental magnetohydrodynamic cored ceramic brick regenerative air preheater. The finite element method was employed for determining both temperature and stress distributions for individual ceramic core bricks at typical cyclic equilibrium operating conditions. Maximum stress values and their locations in the hexagonal core bricks were calculated and compared with values predicted by an earlier, more approximate method as well as with failure modes in an actual preheater. The maximum stresses were found to be circumferential; that is, acting perpendicularly to the direction of the gas flow passages.

CHAPTER I

INTRODUCTION

In the open-cycle magnetohydrodynamic (MHD) system, there is a requirement for combustion intake air at temperatures on the order of 1800°K. One method proposed for accomplishing this involves use of a cored ceramic brick regenerative heat exchanger, or preheater. The operational modes of the preheater are the alternating reheat and blow-down cycles, wherein the preheater core is heated by combustion exhaust gases and cooled by combustion intake air, respectively.

Coal is the fuel proposed for MHD systems under study at Montana State University. The use of coal as fuel results in liquid coal slag being present in the combustion exhaust gases. This causes complications in the operation of the air preheaters due to slag deposition and run-off on the gas flow passage walls and slag saturation of the ceramic core material. An experimental air preheater, the Moderate Temperature Slag Flow Facility (MTSFF) has been constructed at Montana State University to study these problems.

The MTSFF consists of a columnar core of hexagonal ceramic bricks. Surrounding the core is a circular ceramic containment tube, several layers of ceramic insulation, a steel pressure vessel, and a final layer of fiberglass insulation. There is a small air space between the circular containment tube and the hexagonal core. The core bricks are symmetrically drilled with nineteen holes, 19.1 mm. in diameter (see Figures 1a and 1b).

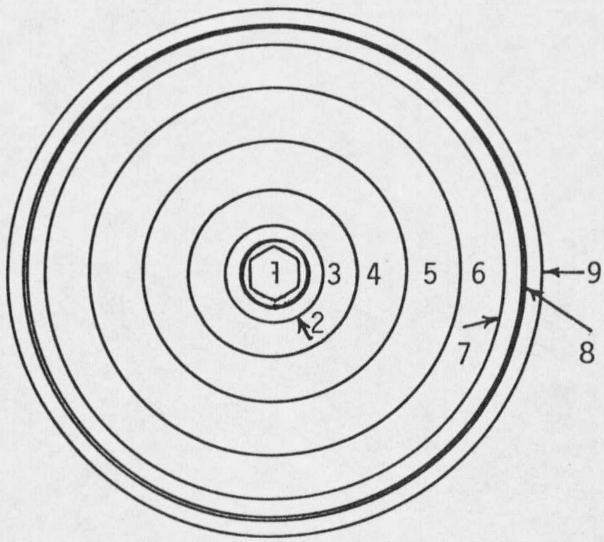

1 - ceramic core
2 - containment tube
3-6 - ceramic insulation
7 - cerafelt blanket
8 - steel shell
9 - fiberglass insulation

Figure 1a MTSFF cross section

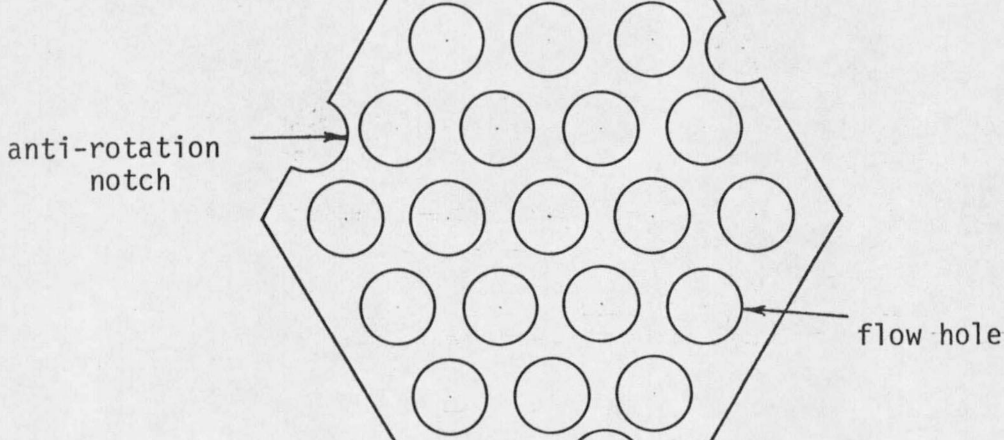

Figure 1b Hexagonal core brick cross section

The primary purpose of this thesis is to investigate thermal stresses in the ceramic core bricks of the MTSFF due to alternate heating and cooling in the reheat and blowdown cycles. Also of interest is the comparison of these predicted stress levels with those predicted by an earlier technique, and the extension of the analysis to a full scale, operational air preheater.

CHAPTER II

LITERATURE REVIEW

Traditionally, analytical methods for evaluation of thermal stress have been limited to simple geometries, for which an analytical solution of the heat conduction equation exists. Upshaw [1], in a MHD air preheater design study used this method by approximating the complex 19-hole cored brick pattern as a bundle of cylindrical tubes. Using this model, he then obtained a quasi-steady-state temperature distribution for heating or cooling of the tubes from their inner surface. Then, by considering the tubes to be of infinite length, he was able to use thermal stress relations presented by Timoshenko and Goodier [2] for free standing infinite cylinders.

An alternative to this problem simplification is the use of numerical methods. Huebner [3] lists the two principal numerical methods for heat transfer and stress analysis as the general finite difference and finite element methods. Both are suitable for solving the corresponding governing equation over a field of interest, but he also points out that the finite difference method becomes increasingly difficult to use for complex geometries or unusual boundary conditions. Huebner [3] and Gallagher [4] both state that the primary advantage of the finite element method is the treatment of complex geometries and boundary conditions. This, in addition to the extensive availability of general purpose finite element computer codes for both heat transfer [5, 6, 7, 8] and stress analysis [8, 9] makes the finite element method an attractive one to use for this problem.

Boundary condition data for heat transfer and stress analysis of the preheater core bricks is readily available. Recent work has been done by Herrick [10] on the thermal simulation of the MTSFF, and experimental data on heat transfer and temperature profiles is also available from operation of the facility.

CHAPTER III

THEORY

Temperature and Stress Fields

Upshaw [1] describes the preheater temperature distribution and, consequently, the thermal stress distribution as consisting of three types. These are the axial and radial temperature distributions extending over the entire preheater body and the localized radial temperature distributions between flow holes. The axial temperature profile is relatively well defined. Figure 2 shows a typical MTSFF axial temperature profile taken from thermocouple data during facility operation. All the data falls within five percent of a linear curve fit. This is significant because a linear temperature distribution of this type will produce no stress in the preheater core [11]. Herrick [10] shows that the axial heat flux at any one point in the preheater core is less than 0.01 percent of the radial heat flux, an insignificant amount. Thus, axial effects can be ignored for both stress and heat transfer calculations.

The remaining two preheater temperature distributions, radial body and localized 'radial', need not be considered separately. They both fall in the same plane, perpendicular to the preheater core axis. Proper selection of core brick boundary conditions will yield a complete combined solution through the finite element analyses.

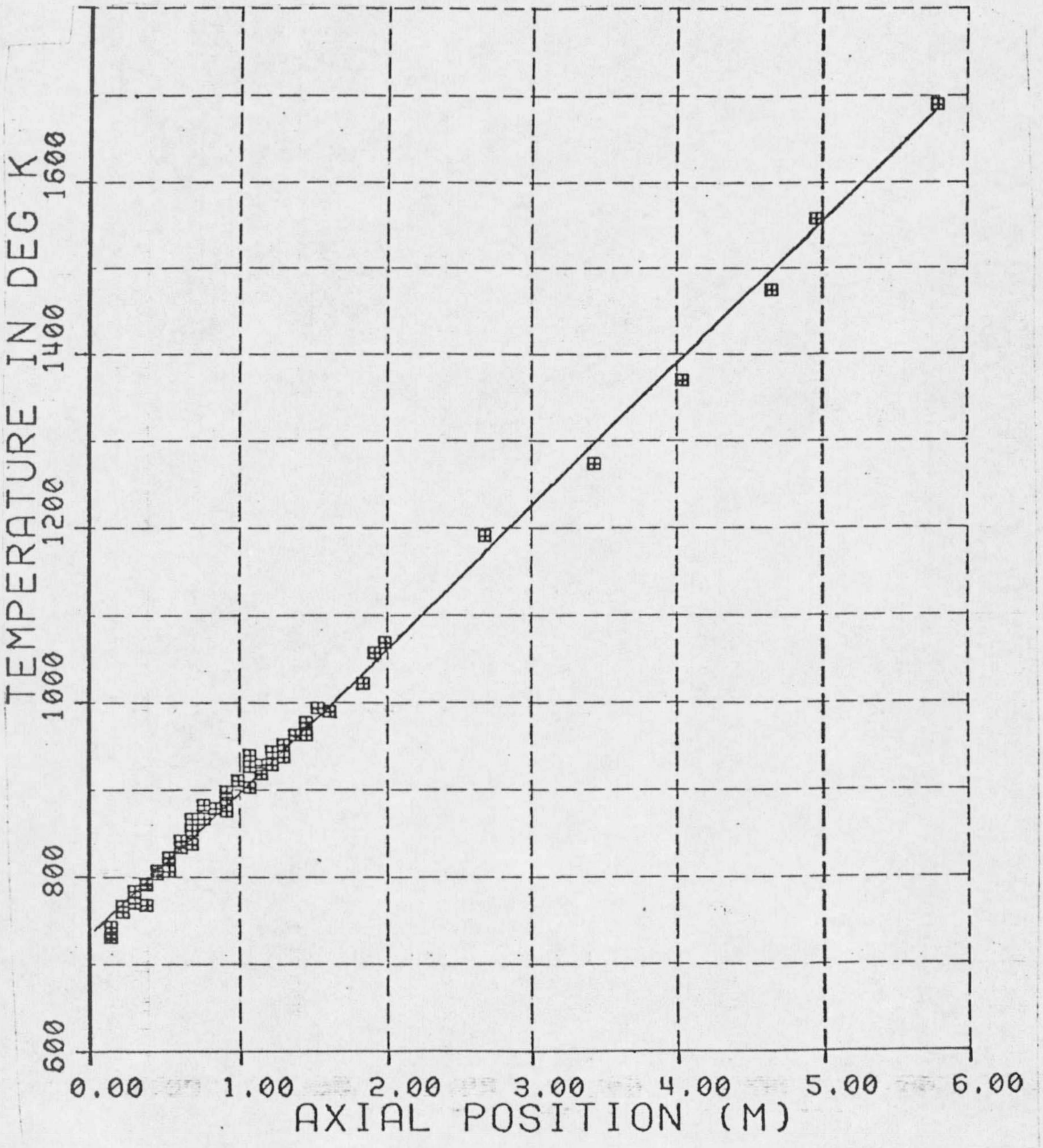

Figure 2 Axial temperature profile
MTSFF

Boundary Conditions

Heat Transfer

The hexagonal core brick (Figure 1b) is drilled symmetrically with 19 holes, 19.1 mm. in diameter with a spacing-to-diameter ratio (S/D) of 1.42. These holes form the gas flow passages, or flow holes. Immediately adjacent to the core are six air spaces formed by the fit of the hexagonal core bricks in the circular containment tube. The containment tube is surrounded by ceramic insulation brick, a steel shell, and a final layer of fiberglass insulation.

Heat transfer occurs at the flow-hole surfaces by forced convection and at the core brick perimeter by radiation and free convection. During reheat, the hot combustion exhaust gas in the flow holes transfers heat to the core bricks, increasing their temperature. While in blowdown, the cooler counterflow gases in the flow holes remove heat from the core bricks, decreasing brick temperatures. When the average brick temperature changes during reheat and blowdown sum to zero, the preheater is considered to have reached cyclic equilibrium. Heat transfer between the MTSFF core brick perimeter and the adjacent containment tube falls into two categories; natural convection and radiation, with radiation predominating. In a full scale heat exchanger, where identical core brick columns would be packed closely together, the brick perimeters could be considered adiabatic for all but the outermost brick edges.

Ceramic-gas heat transfer in the flow holes is calculated from the equation:

$$q_f = h_f (T_c - T_g) \tag{1}$$

where q_f = heat flux from gas to ceramic core brick (W/m^2),

h_f = flow hole convective coefficient (W/m^2-°K),

T_c = ceramic surface temperature (°K), and

T_g = gas temperature (°K).

Herrick [10] used the following correlations for the convective coefficient:

$$Nu = 0.131 [Re^{2/3} - 138] Pr^{1/3} [1 + \frac{1}{3} (\frac{D}{Z})^{2/3}] (\frac{f_r}{f_o})^{0.914} \tag{2a}$$

$$h_f = Nu\ D\ K_g$$

where: Re = local Reynolds number,

Pr = local Prandtl number,

D = flow hole diameter (m),

Z = distance from flow hole entrance (m),

f_r = Darcy-Weisbach friction factor for rough pipe,

f_o = Darcy-Weisbach friction factor for smooth pipe, and

k_g = local gas thermal conductivity (W/in-°K).

He also used the following correlation for friction factors:

$$\frac{1}{\sqrt{f}} = 1.74 - 2 \log_{10} [\frac{ks}{D} + \frac{18.7}{Re\sqrt{f}}] \tag{3}$$

where: f = Darcy-Weisbach friction factor,

k_s = equivalent sand grain roughness, and

Re = local Reynolds number.

The radiant heat transfer between the core brick perimeter and the containment tube can be calculated from a simplified zonal analysis. Herrick [10] shows that the containment tube is isothermal to within 1°K over the entire reheat and blowdown cycles at any one axial position. He also shows that the core brick perimeter temperature varies by less than one percent at any one axial position or point in time. Thus, the two surfaces can be considered isothermal. Assuming grey, diffuse emissive properties, the radiosities of the two surfaces can be calculated as given by Ozisik [12].

$$R_i = \varepsilon_i \sigma T_i^4 + \rho_i \sum_{j=1}^{N} R_j F_{i-j} \tag{4}$$

where: R_i = radiosity of surface i,

σ = Stephan-Boltzmann constant,

ε_i = emissivity of surface i,

T_i = temperature of surface i,

N = number of surfaces,

$\rho_i = (1 - \varepsilon_i)$, and

F_{i-j} = view factor from surface i to surface j.

The view factors from the brick perimeter (surface 1) can be evaluated by inspection. See Figure 3.

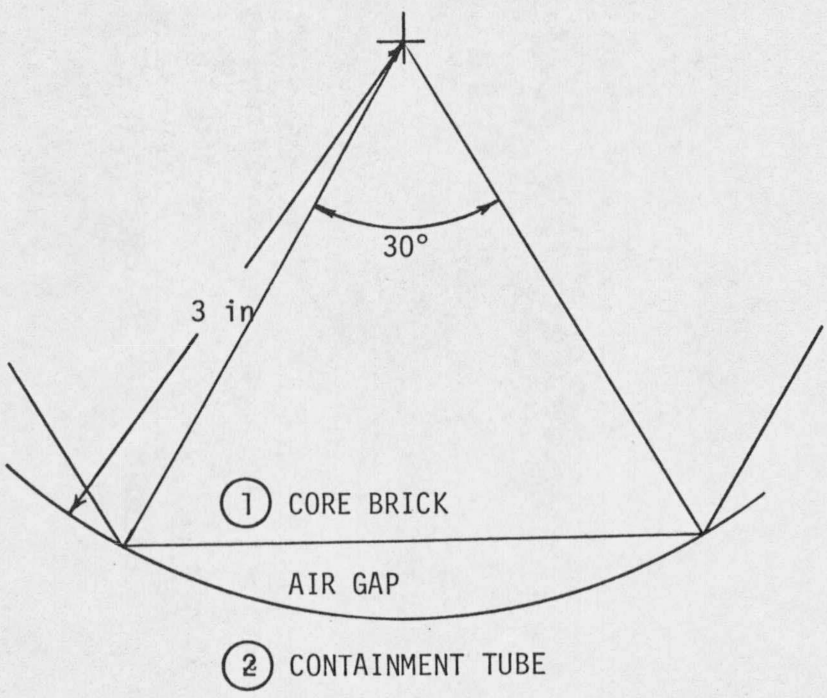

Figure 3 Core brick perimeter radiant zonal analysis

$$F_{1-1} = 0$$

$$F_{1-2} = 1$$

Applying the theorem of view factor reciprocity yields the view factor for the containment tube (surface 2).

$$F_{2-2} = 0.045$$

$$F_{2-1} = 0.955$$

To simplify the analysis, with little effect on the accuracy, these last two view factors can be approximated:

$$F_{2-2} = 0$$

$$F_{2-1} = 1$$

This is equivalent to infinite parallel plates. Substituting the chosen view factors into (4) and solving for R_1 and R_2:

$$R_1 = (\varepsilon_1 \sigma T_1^{\,4} + \rho_1 \varepsilon_2 \sigma T_2^{\,4})/(1 - \rho_1 \rho_2) \quad (5a)$$

$$R_2 = (\varepsilon_2 \sigma T_2^{\,4} + \rho_2 \varepsilon_1 \sigma T_1^{\,4})/(1 - \rho_1 \rho_2) \quad (5b)$$

The heat flux from each zone is given by Ozisik [12]:

$$q_i = R_i - \sum_{j=1}^{N} R_j \, F_{i-j} \quad (6)$$

where: q_i = heat flux from surface i.

Substitution of (5) into (6) and solving for q_1 and q_2 gives:

$$q_1 = - q_2 = \sigma(T_1^4 - T_2^4)/(1/\varepsilon_1 + 1/\varepsilon_2 - 1) \quad (7)$$

It should be noted that the finite element computer code utilized is not capable of handling radiant heat transfer. It does, however, have provisions for convective heat transfer. It is necessary to express the radiant heat transfer as an equivalent convective condition, by means of an equivalent radiative coefficient. This can be done with little error, providing the difference between T_1 and T_2 is small. Herrick [10] shows that this difference is less than five percent at any one time or position. Therefore:

$$(T_1^4 - T_2^4) \doteq 4\, T_2^3(T_1 - T_2) \quad (8)$$

Substitution of (8) into (7) gives:

$$q_1 = [4\sigma T_2^3/(1/\varepsilon_1 + 1/\varepsilon_2 - 1)](T_1 - T_2) \quad (9)$$

which is in the form of (1) if the equivalent radiative coefficient at the core brick perimeter is defined:

$$h_r = 4\sigma T_2^3/(1/\varepsilon_1 + 1/\varepsilon_2 - 1) \quad (10)$$

The containment tube temperature, T_2, must be used in place of a gas temperature.

In addition to the radiative heat transfer between the core bricks and containment tube, natural convective heat transfer occurs. This can be approximated from an empirical correlation given by Jakob [13] for natural convection between isothermal walls.

The Nusselt number, Nu_δ, for natural convection in a vertical gap is defined:

$$Nu_\delta = h_c \delta / k_{g_p} \qquad (11)$$

where: k_{g_p} = gas thermal conductivity (W/m-°K),

h_c = convective coefficient (W/m^2-°K), and

δ = average gap width (m.).

The Nusselt number is a function of the Grashof number, Gr_δ, for heat transfer in vertical enclosures. The Grashof number is defined:

$$Gr_\delta = \rho_g{}^2 g\beta \; (T_1 - T_2) \; \delta^3/\mu^2 \qquad (12)$$

where: ρ_g = gas density (Kg/m^3),

g = gravitational acceleration (m/sec^2),

β = volume coefficient of expansion for an ideal gas (°K^{-1}),

T_1 = temperature of wall 1 (°K),

T_2 = temperature of wall 2 (°K), and

μ = dynamic viscosity (Nt-sec/m^2).

The Grashof number does not exceed 2000 at any axial position in the MTSFF air gap. Jakob [13] gives the following as the proper Nusselt number correlation.

$$Nu_\delta = h_c \delta / k_g = 1 \tag{13}$$

This is actually pure conduction. The corresponding heat flux is

$$q_w = h_c \ (T_1 - T_2) \tag{14}$$

where: q_w = convective heat flux at the core brick perimeter (W/m^2).

The total convective coefficient for heat transfer from the core brick perimeter to the containment tube is obtained by summing the natural convective and equivalent radiative terms:

$$h_T = h_c + h_r \tag{15}$$

where: h_T = total perimeter convective coefficient.

Due to symmetry, a thirty degree segment of the core brick can be selected for analysis. The sectioning lines are along adiabatic surfaces. Figure 4 depicts the segment studied and the heat transfer boundary conditions. Note that the segment chosen does not have one of the anti-rotation notches shown in Figure 1b. The anti-rotation notches were ignored throughout the work done for this thesis.

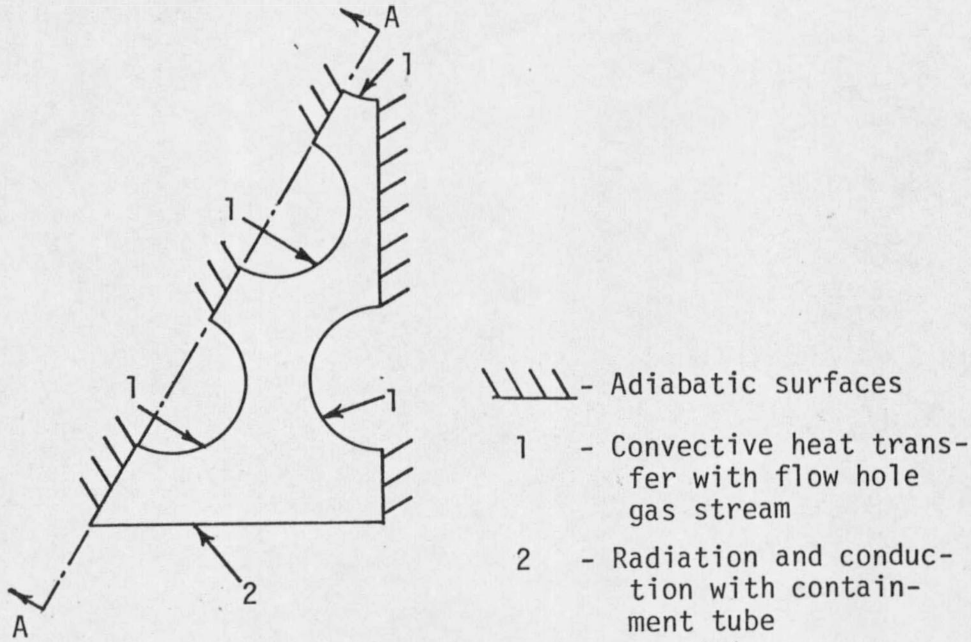

Figure 4 30° segment with thermal boundary conditions

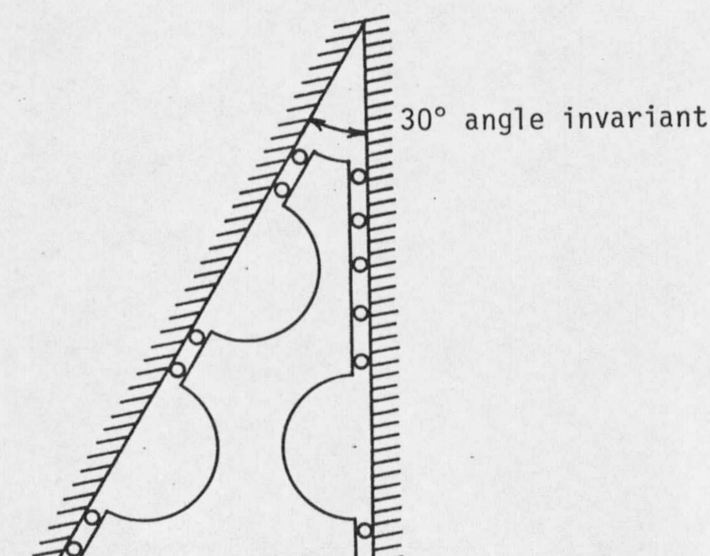

Figure 5 Physical boundary conditions

Physical Boundaries

The core brick surfaces are considered to be free of stress tractions. The bricks are fitted loosely into the containment tube so that there is no binding between them. The average core temperature and containment tube temperature differ by less than four percent at any one axial position. Since both the core and containment tube have similar thermal expansion characteristics, it is assumed that there is no constraint of expansion during operation. The differential pressure between the flow-hole gases and the brick perimeter is negligible as is the axial pressure due to the weight of the column of bricks. This latter is less than .20 MPa at any axial location.

Selection of only one thirty-degree segment of core brick for analysis requires one special physical restraint. For compatibility of motion between segments, the segment angle must remain at 30 degrees and the segment sectioning lines must remain straight. This is accomplished by constraining the points along the sectioning lines to move in a radial direction (see Figure 5).

The Finite Element Method

The finite element method is a means of obtaining an approximate solution to a general governing equation over a specific physical field. The governing equations would be the conduction equation for heat transfer or a suitable equation for stress analysis. The solution obtained is a piecewise, numerical one. The field is divided into a discrete number of finite elements. Within each of these smaller fields, the governing equations are again applied, but with simplifying assumptions. These assumptions might be of a linear temperature distribution or a state of constant strain within the element. The end result of this discretization and simplification is a set of simple, usually linear, equations describing the conditions within each element. Simultaneous solution of these sets of equations produces the overall solution.

The work of the analyst, when using finite elements, is to construct the finite element mesh, and specify boundary conditions. The mesh consists of a set of nodal points, scattered throughout the field. The finite elements are then constructed between the nodal points. The simplest planar element, the triangle, was used in this work. In a triangular element, nodal points serve as the element corners, each nodal point serving one or more element.

The solution is usually in the form of a set of values for each specific nodal point. This would be a set of nodal point temperatures for heat transfer or nodal point displacements and element centroid stress conditions for stress analysis. It should be noted that due to the large number of elements, and the simplifying assumptions within each element, the solution must be considered approximate, not exact. However, the total solution, in general, is a good approximation even if it is not exact for each element.

Computer Codes

Five separate computer codes were used in the work for this thesis. Two were minor, serving only to speed data input to the other three. Of these last three codes, two were modified forms of available finite element heat transfer and stress analysis codes. The third was written by the author to automate the element mesh generation for the thirty degree core brick segment (see Figure 6). The two finite element programs and explanations of the modifications made to each are as follows.

Heat transfer calculations were performed with the code, HEATRANS, written by Edward L. Wilson at the University of California, Berkeley. Wilson and Nickell [5] explain its development. A variational approach is applied to the transient heat conduction problem. The temperature field within the finite elements is approximated by first order polynomial expansion in terms of the nodal point temperatures. The resultant set of first order, ordinary differential equations are then solved with a unique numerical method of assured stability. Modifications made to HEATRANS were in the data input and output methods to allow for a non-constant initial temperature distribution, and speed the data transfer to storage files. The remainder of the program was unchanged.

Stress level calculations were performed with a modified version of PALOS, a computer code developed by Wilson et al. at the University of

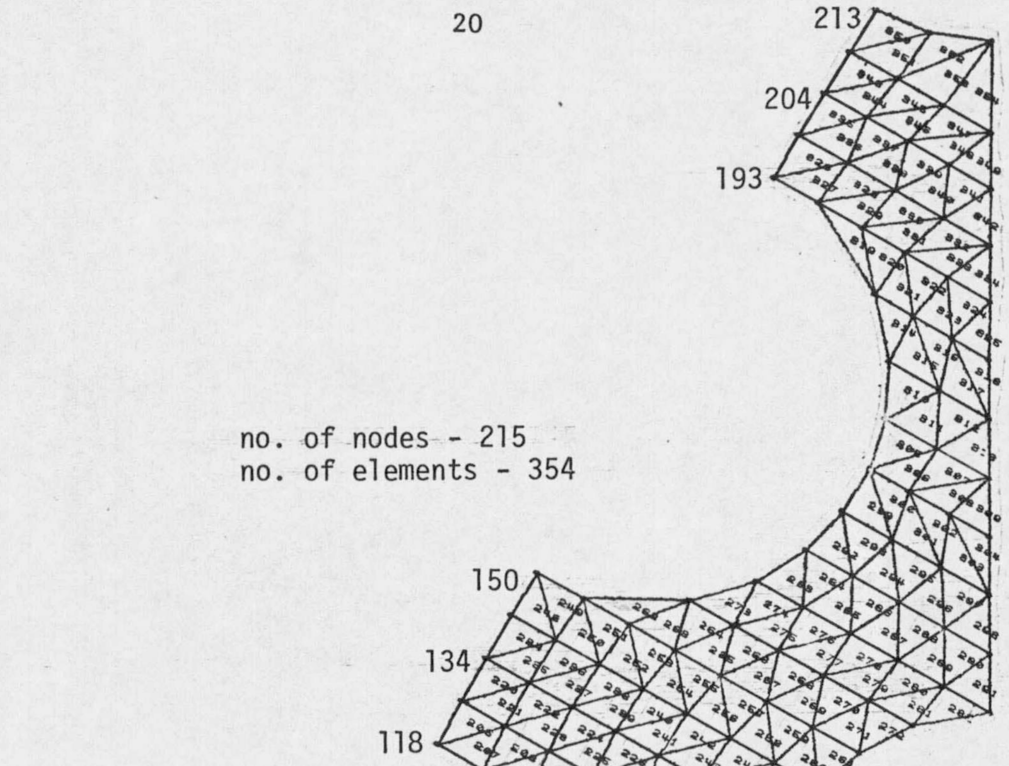

scale 3.17:1

Figure 6 Finite element mesh

California, Berkeley. The program development is explained by Goodreau [9]. Variational calculus is used to minimize the potential energy for a linear elastic body, which is discretized by a finite element mesh. Displacement within each element is approximated by a Ritz linear polynomial expansion in terms of the displacements of the nodal points. This results in constant strain and stress states within the element. The assembled set of linear equations are solved by Gaussian elimination. Modifications made to PALOS were solely in data input methods.

Application of Computer Codes

Heat Transfer

HEATRANS is capable of performing transient heat transfer analyses from an initial temperature distribution and specified temperature and heat flux boundary conditions. It was utilized as follows:

For one axial position:

(1) The end of reheat (EOR) average core temperature was determined from MTSFF experimental data, Figure 7a. This was used as the blowdown initial temperature.

(2) The average gas-ceramic temperature difference for blowdown was determined from Herrick's [10] work and used to determine the average blowdown gas temperature, T_{gb} (see Figure 7b). The containment tube temperature was chosen as the average of end of reheat (EOR) and end of blowdown (EOB) core temperatures as

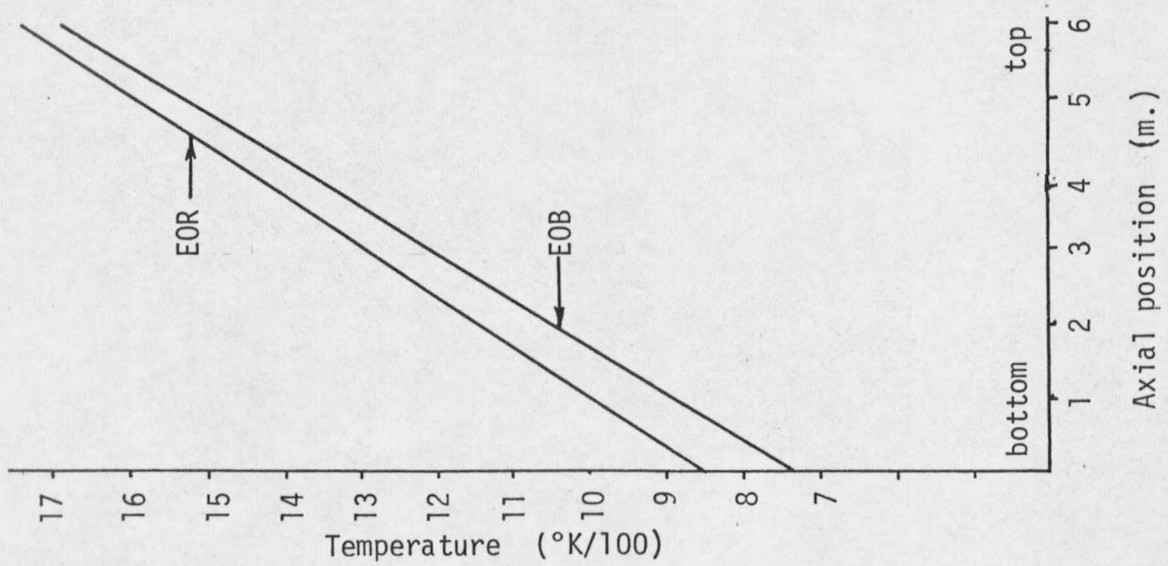

Figure 7a Average ceramic core temperatures - MTSFF (actual)

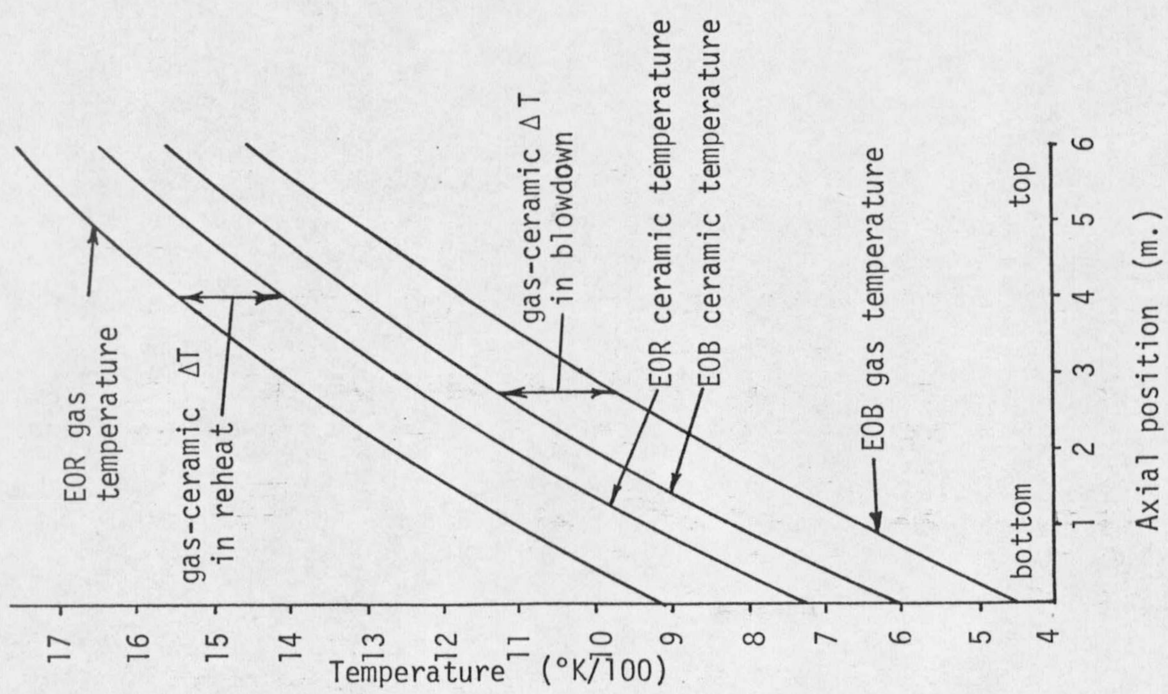

Figure 7b Gas and ceramic temperatures from Herrick [10]

in Herrick's [10] results. And convective coefficients for the flow holes and the brick perimeter were calculated from equations (2) and (15).

(3) Using data determined in 1 and 2 above, HEATRANS was used to calculate the EOB temperature distribution.

(4) New thermal boundary conditions were calculated similarly to 2, above, for reheat.

(5) HEATRANS was used to calculate the EOR temperature distribution from the data determined in 4, and using the EOB temperature from 3, above, for the initial distribution.

(6) The cycle, 2-3-4-5, was carried out until cyclic equilibrium was achieved. The one change in the outlined procedure was the use of the EOR temperatures from (5) for the initial temperatures for (2). Cyclic equilibrium was considered achieved when two successive EOR temperature distributions were within 0.5°K of each other.

(7) Temperature distributions were calculated at 10 sec. intervals for the complete blowdown-reheat cycle.

Considerable leeway, up to 5°K, was allowed as far as duplication of actual MTSFF average EOR and EOB core temperature was concerned. This was due to the fact that thermal stress values are dependent on relative temperature differences, not actual temperatures.

Stress Analysis

Two types of planar stress analysis were available from PALOS. These were the approximations of plane strain and plane stress. Plane strain is an approximation wherein the strains acting perpendicularly to the plane of analysis are set identically to zero. This technique is most useful for analyses of long, theoretically infinite bodies acted upon by loads with no component in the long, axial direction. Little [14] discusses this technique in considerable detail. In the plane stress approximation, the stresses acting perpendicularly to the plane of analysis are set identically to zero. This technique is primarily intended for analyses of plane plates of small constant thickness acted upon by forces only in the plane of the plate. The core brick, three inches in axial length and six inches across, fits neither the state of plane stress nor plane strain exactly. It is, however, most well-suited to the plane stress analysis. This is due to its length to width ratio of 0.5 and the low level of axial compression, less than 0.20 MPa. This choice of plane stress analysis is supported by conditions in the MTSFF core, dismantled after 1100 hours operation. The core bricks were extensively cracked and broken from stresses acting in the circumferential direction, while unbroken from axial stresses. Therefore, the stress calculations performed with PALOS utilized the approximation of plane stress.

Application of PALOS required input of a temperature distribution as determined by HEATRANS, and suitable material properties.

CHAPTER IV

RESULTS

Analysis Conditions

Temperature and thermal stress distributions were calculated for the MTSFF core bricks by application of the finite element codes. Three cases of thermal conditions were studied. Cases 1 and 2 duplicated typical operating conditions for two locations in the MTSFF core. Case 1 was located 3.35 m. from the core bottom in a highly cracked zone of MTSFF core bricks; revealed upon inspection after 1100 hours at operating conditions. Case 2, at 0.05 m. was chosen to provide a comparison for Case 1. Case 3 used the same flow conditions as Case 1, but the brick perimeter was made adiabatic to simulate a center brick in a large preheater. The finite element mesh utilized is shown in Figure 6. The gas and containment tube temperatures, convective coefficients, and ceramic physical properties used for the three cases are tabulated in Table 1.

Figures depicting results are as follows. Core brick thermal profiles for selected times during reheat and blowdown are shown in Figures 8-10. Thermal stress distributions for some selected thermal profiles are depicted in Figures 11-16.

Thermal Behavior

The core brick temperature profiles for all three cases were found to possess similar characteristics at corresponding cycle times. The profiles, depicted in Figures 8-10, result from the characteristics of

TABLE 1. Thermal/Physical Data

Property	Case 1	Case 2	Case 3
Ceramic Thermal Conductivity (W/m-°K)	2.95	3.96	2.95
Ceramic Density (kg/m^3)	3170	3240	3170
Ceramic Specific Heat (J/Kg-°K)	1160	1080	1160
Containment Tube Temperature (°K)	1315	800	--
Brick Perimeter Convective Coefficient (W/m^2-°K)	190	47	0
Flow Hole Gas Temperature Reheat/Blowdown (°K)	1395/1175	945/600	1395/1175
Flow Hole Convective Coefficient Reheat/Blowdown (W/m^2-°K)	56/50	62/67	56/50
Blowdown Duration (sec.)	240	240	240
Reheat Duration (sec.)	360	360	360
Gas Flow Rate (for 19 holes) Reheat/Blowdown (Kg/hr)	180/170	180/170	180/170
Ceramic Young's Modulus (MPa)	1.1×10^5	1.1×10^5	1.1×10^5
Ceramic Poisson's Ratio	0.2	0.2	0.2

Sources for non-derived data are listed in the Appendix.

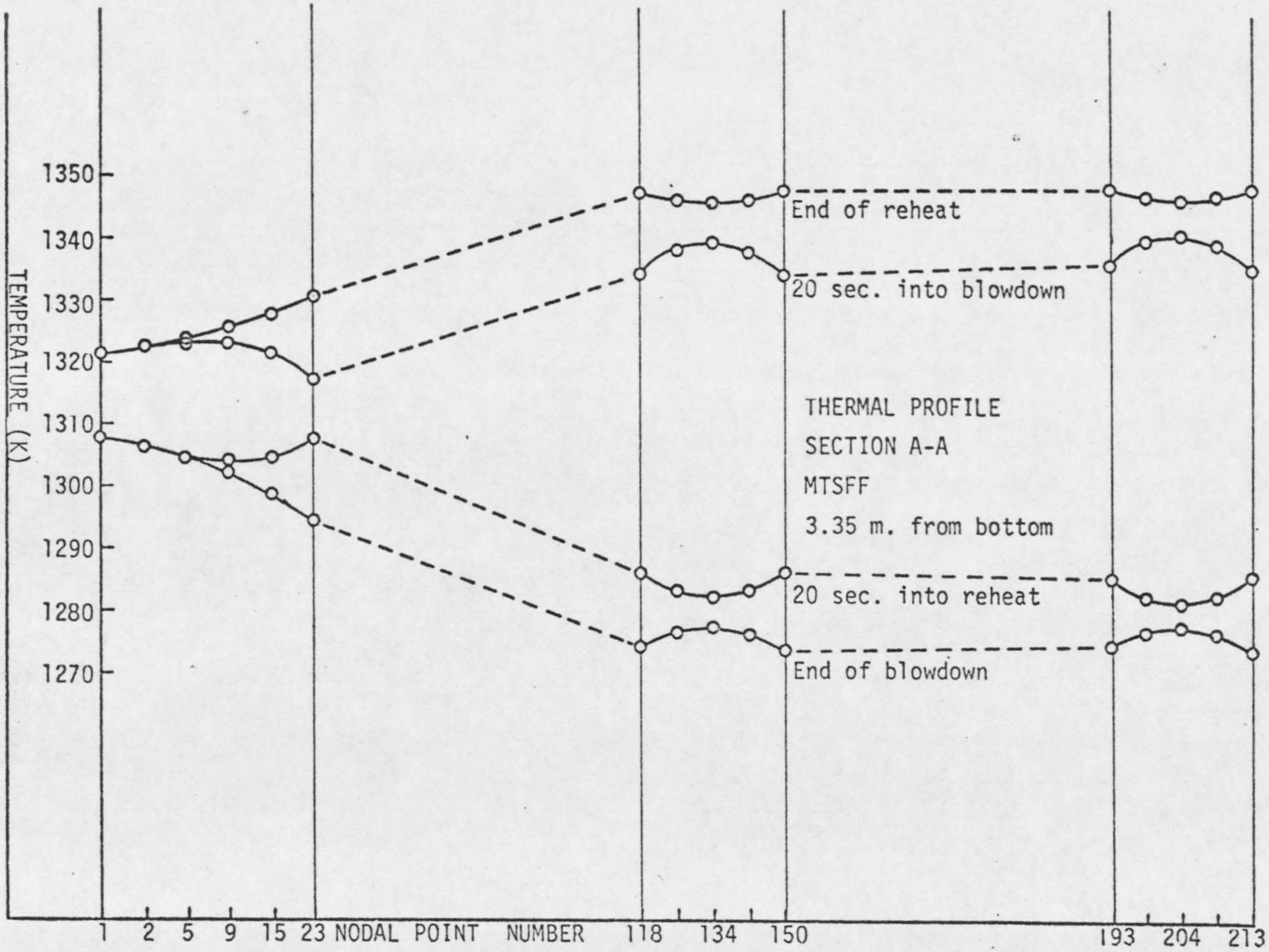

Figure 8 Temperature distribution for Case 1

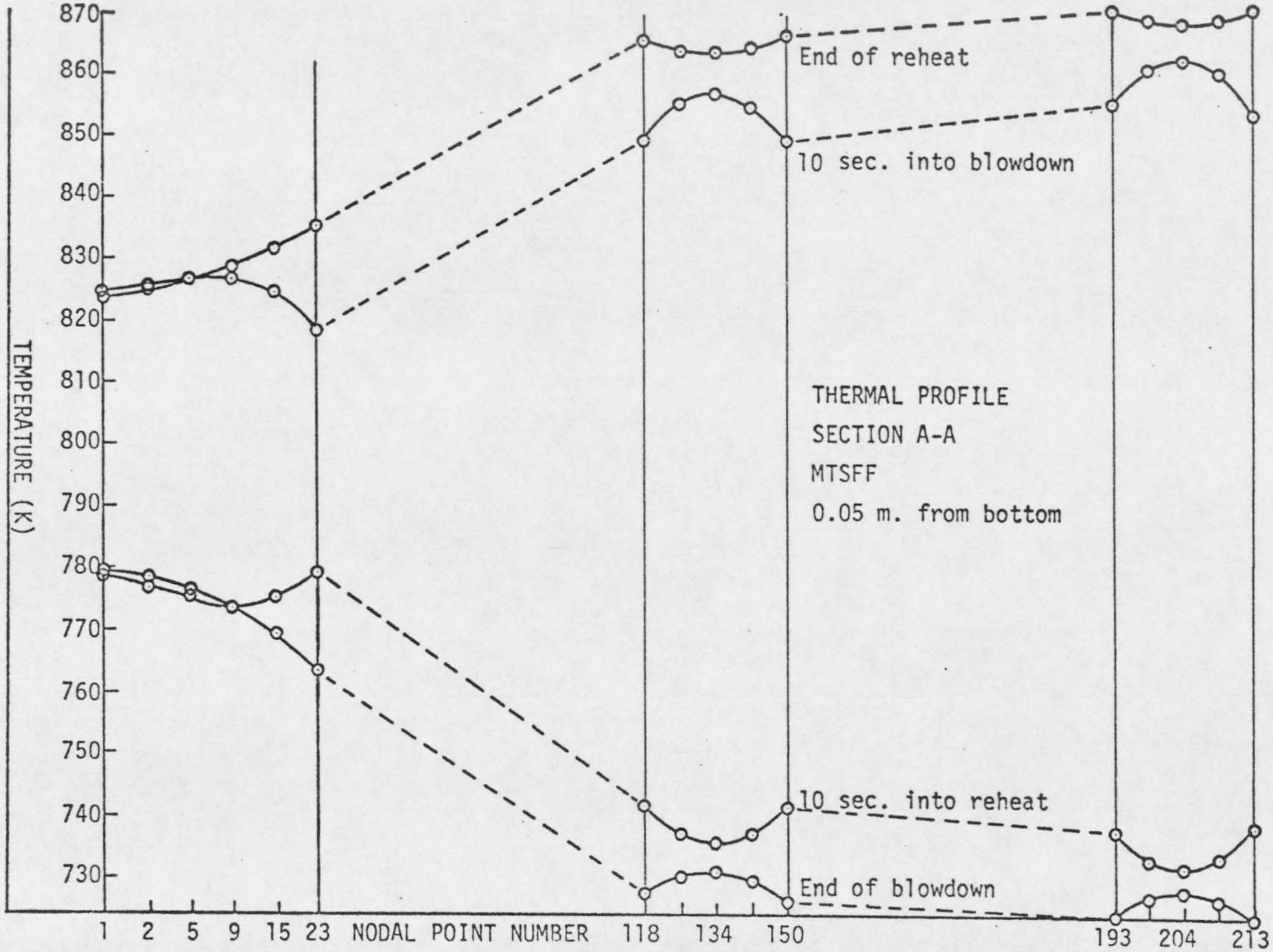

Figure 9 Temperature distribution for Case 2

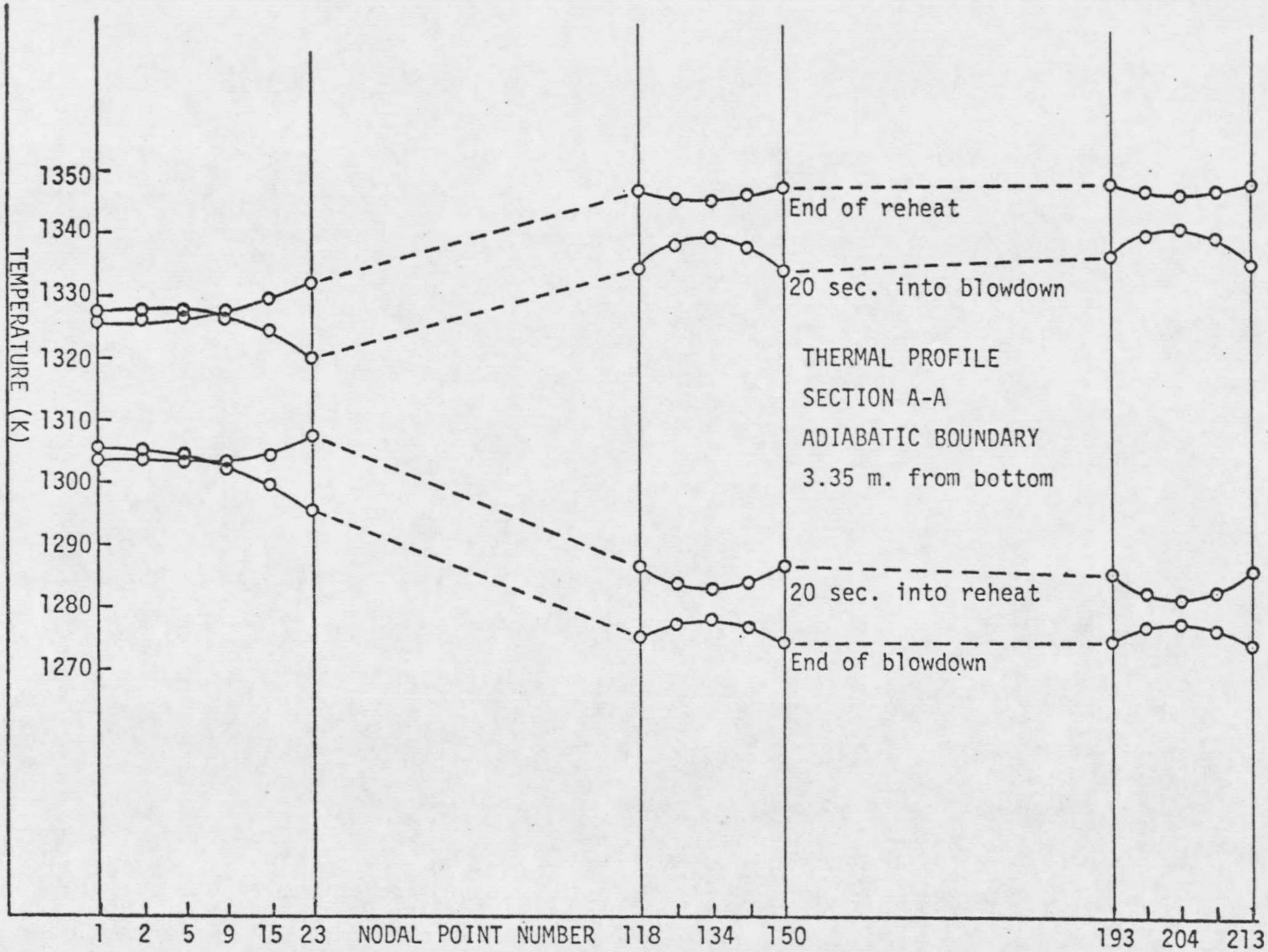

Figure 10 Temperature distribution for Case 3

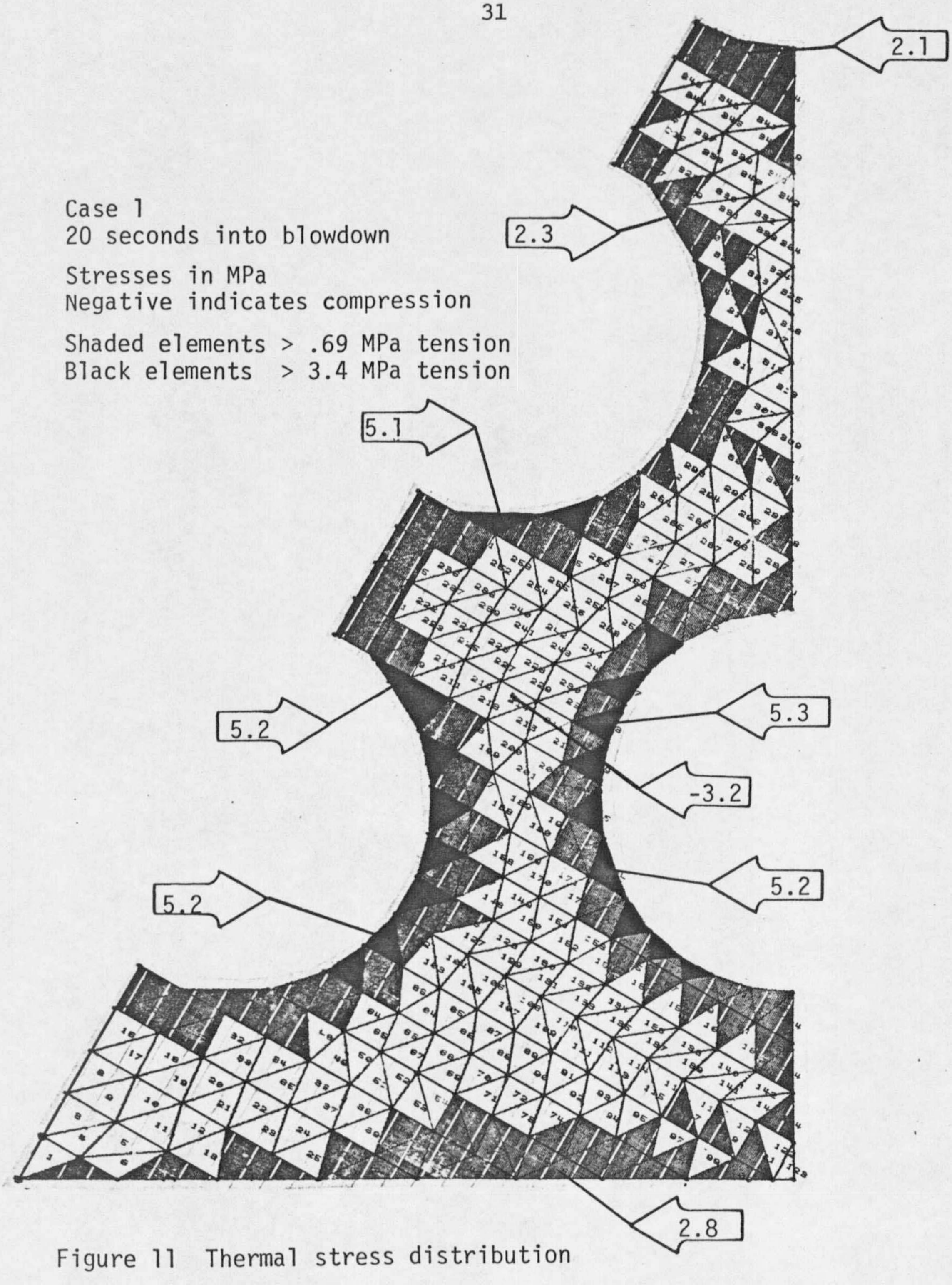

Figure 11 Thermal stress distribution

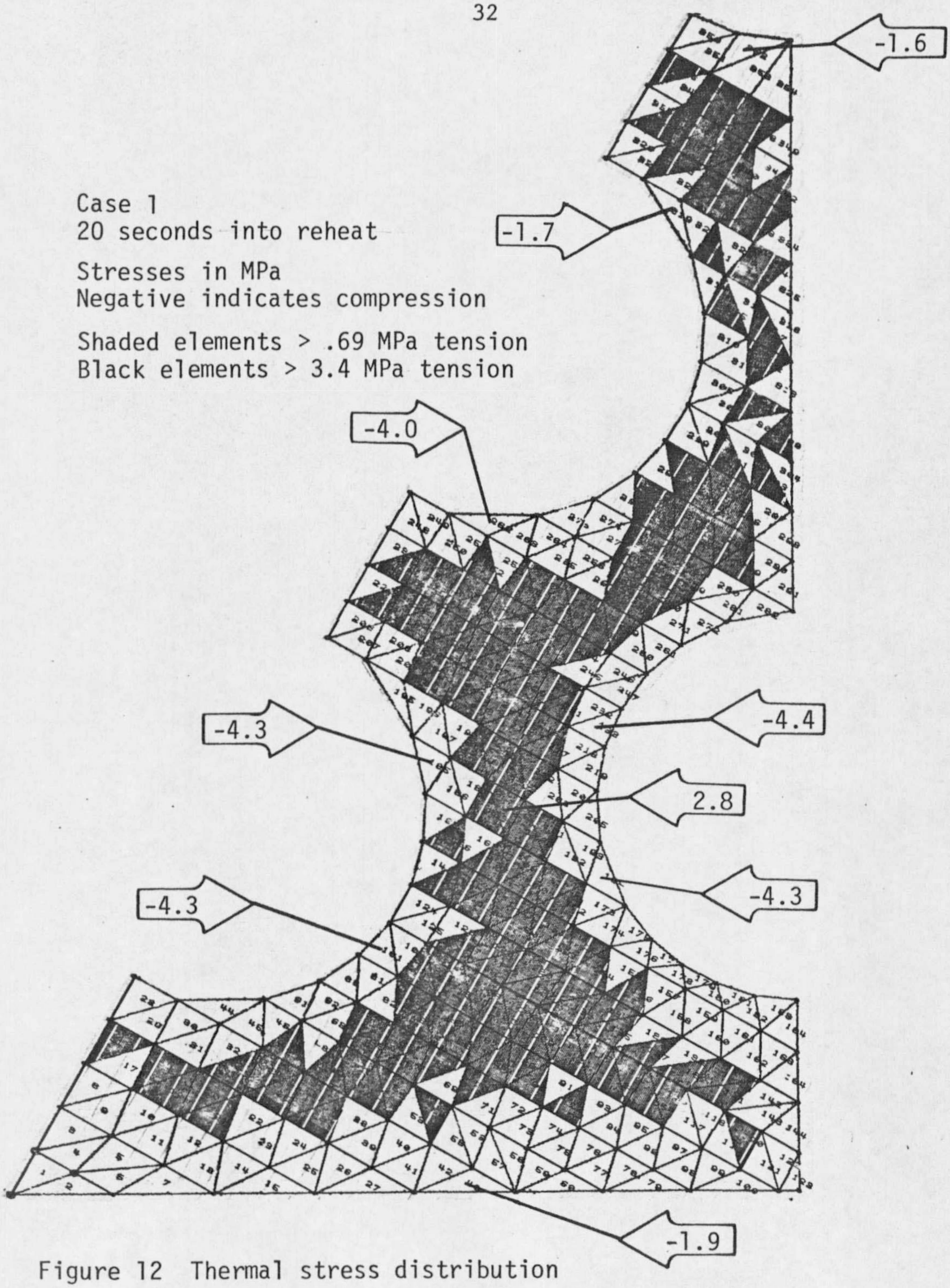

Figure 12 Thermal stress distribution

Case 2
10 seconds into blowdown

Stresses in MPa
Negative indicates compression

Shaded elements > .69 MPa tension
Black elements > 3.4 MPa tension

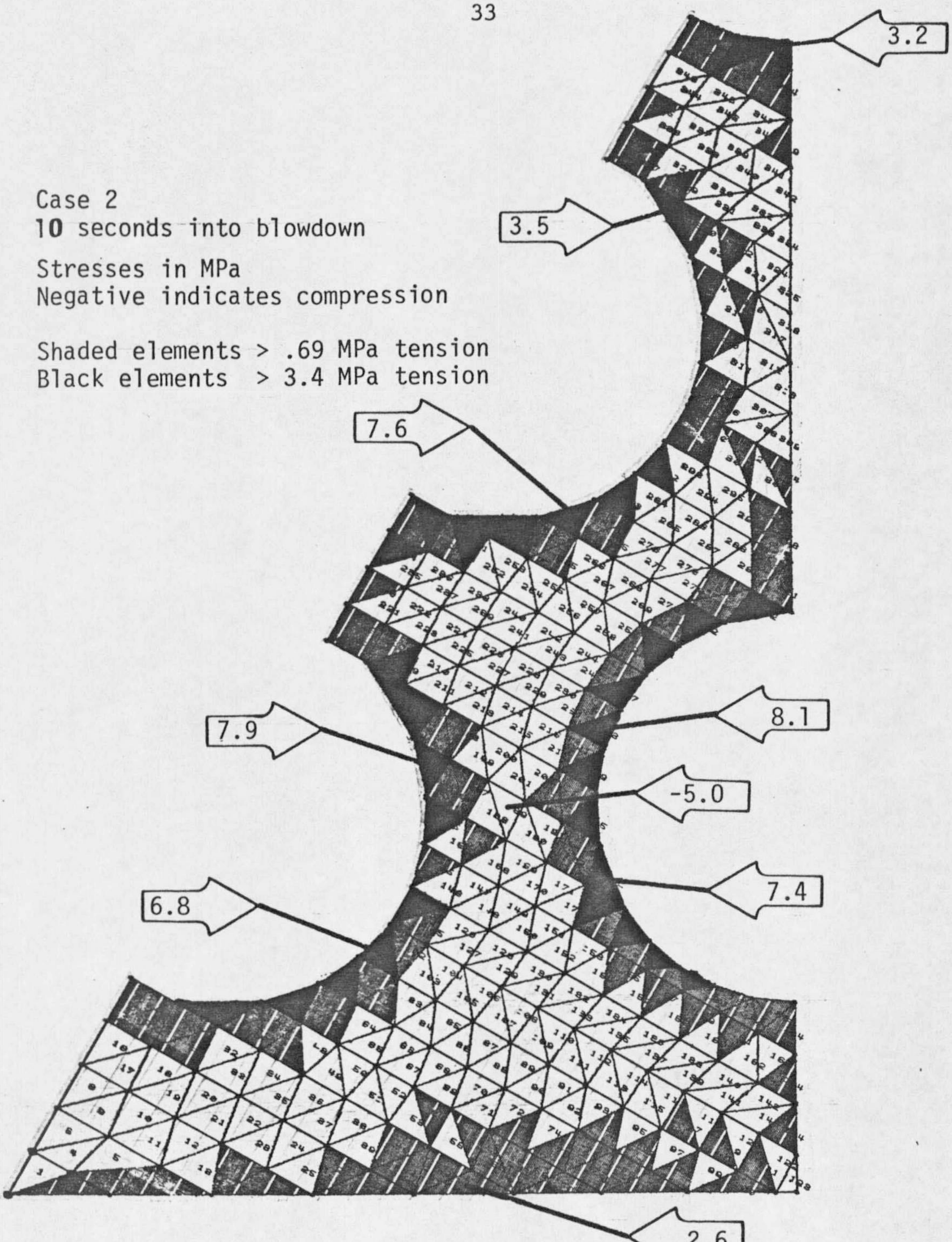

Figure 13 Thermal stress distribution

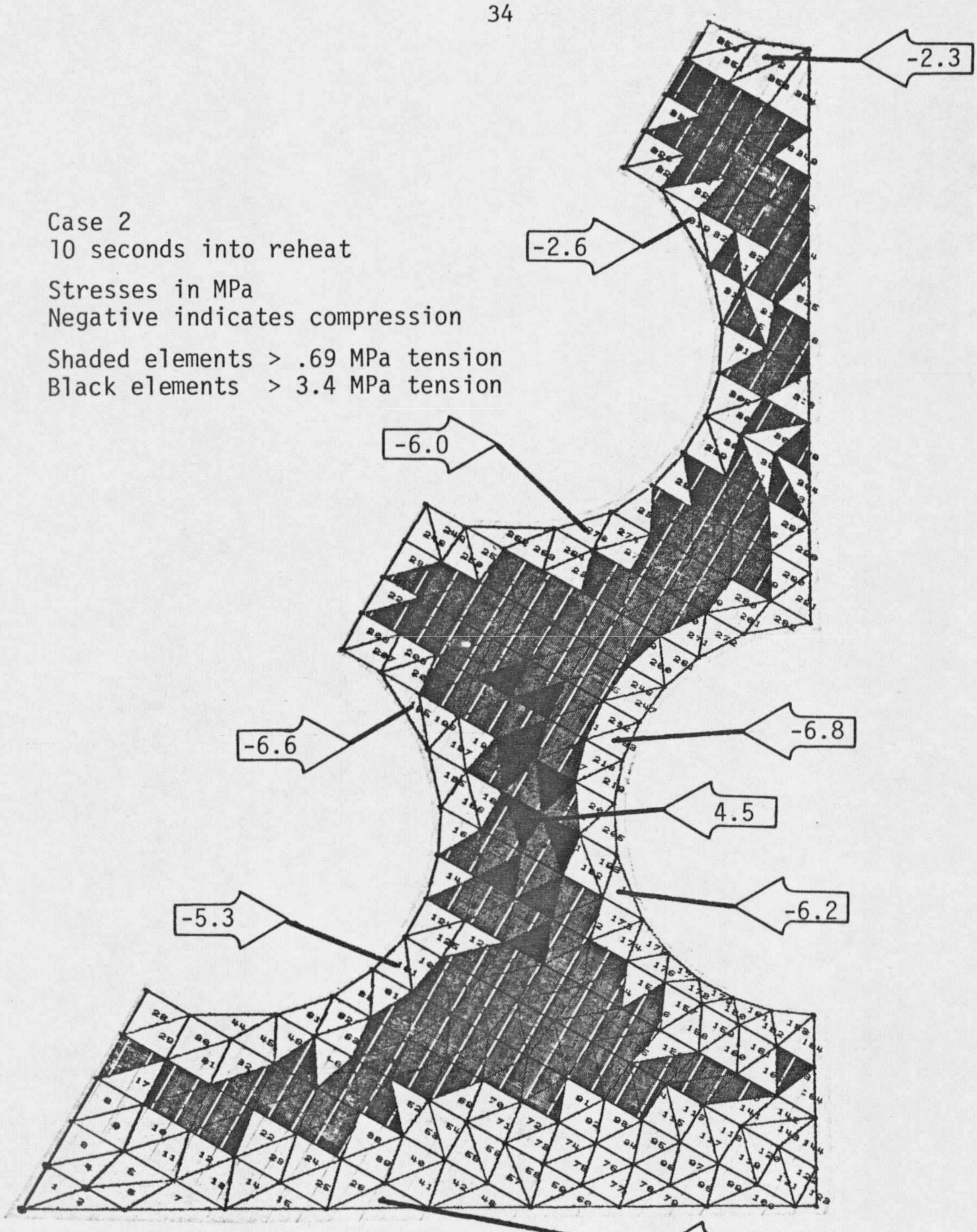

Figure 14 Thermal stress distribution

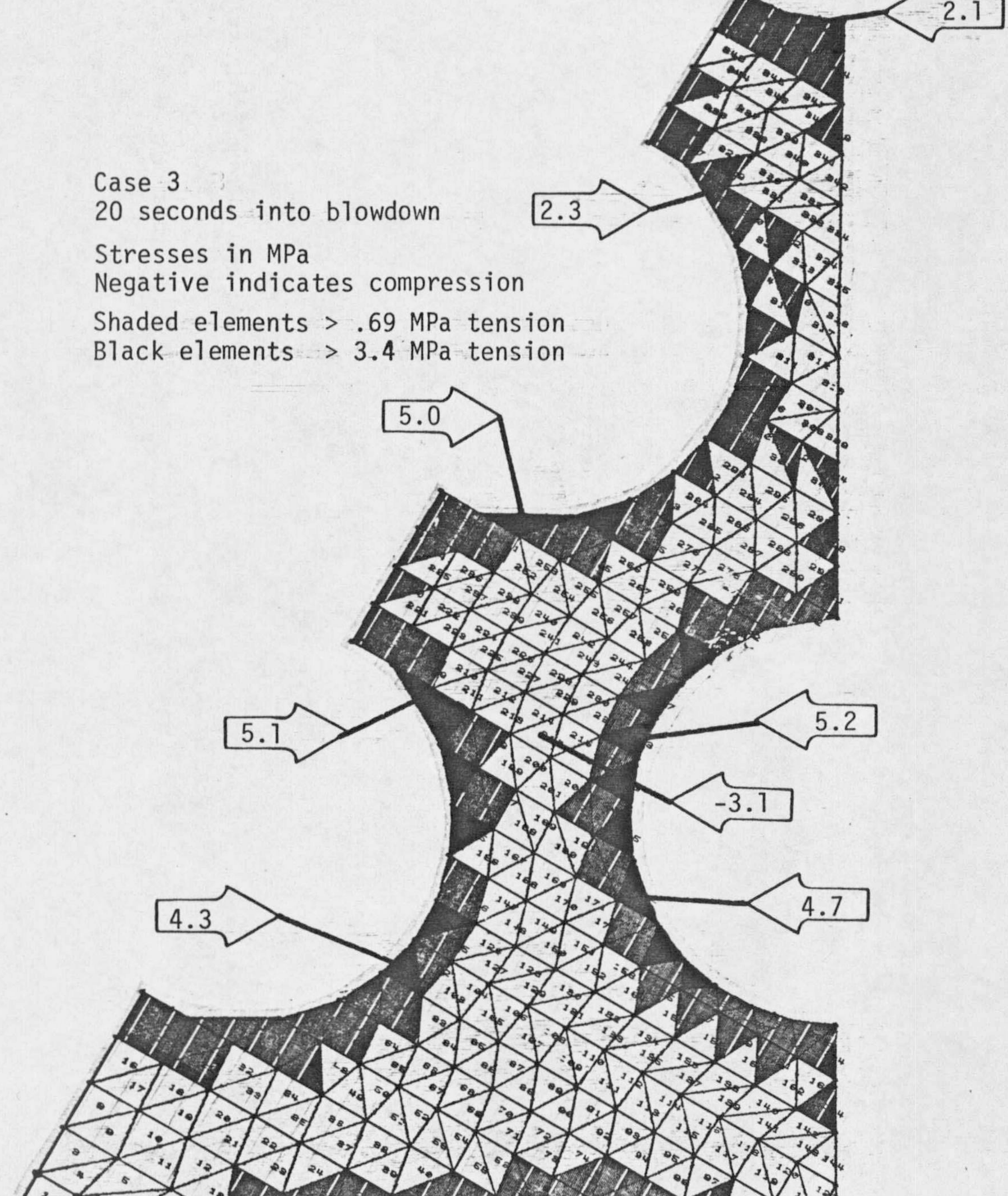

Figure 15 Thermal stress distribution

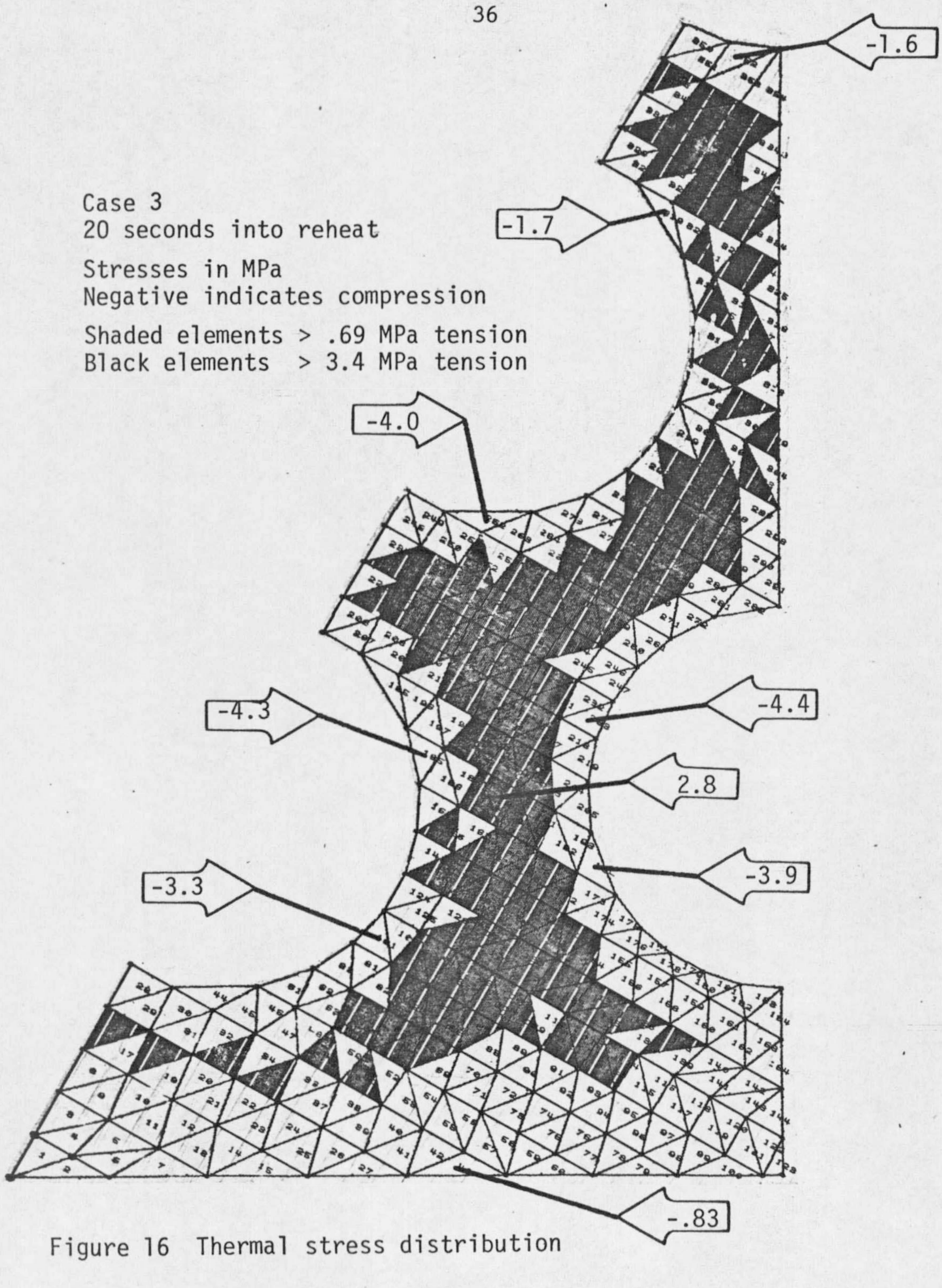

Figure 16 Thermal stress distribution

two types of temperature distributions. The behavior of the first type, localized "radial", is seen at flow hole edges; specifically at nodal points 118-150 and 193-213 in the figures. The second type is the overall "body" distribution, resulting from heat flow between the brick center and the brick perimeter. This is seen as the large temperature difference between nodes 1 and 118. The effect of the localized "radial" temperature distribution can also be seen in the sharp curvature of some of the thermal profiles between nodes 9 and 23.

The differences between individual cases were small, being of two types. The first was a large difference in cyclic temperature oscillation between Case 1 and Case 2. Case 1, 3.35 m. from the bottom, had an average temperature change of 60°K between reheat and blowdown cycles. Case 2, at 0.05 m. from the bottom, had an average change of 100°K. The second type of difference was in the slope of the temperature profile at the brick perimeter, node 1. The slope, zero in the adiabatic Case 3, was non-zero in the corresponding Case 1. This is as expected. Other than these differences, the temperature profiles of all three cases were of similar form.

Thermal Stresses

It was found that peak thermal stresses occurred at the location and instant of maximum curvature of the localized temperature distribution. This occurred early in both reheat and blowdown cycles, within 10 to 20 seconds of beginning the cycle. During blowdown, the maximum tensile stresses were circumferential, located at the flowhole surfaces. The maximum compressive stresses were lower in magnitude, and located in the brick interior, between flow holes. During reheat, this situation was reversed, with compressive surface stresses and tensile interior stresses; compressive stresses being greater. Blowdown stresses were greater than reheat stresses for a given case due to greater temperature profile curvature. Since the brittle Corhart RFG core material is weaker in tension than compression, it is the blowdown tensile stresses that are of primary interest.

Figures 11-16 depict stress distributions for cases 1-3 at the moments of maximum stress. Elements in which the maximum stress was greater than .690 MPa tension are shaded grey. Elements with maximum stress greater than 3.45 MPa tension are solid black. Arrows indicate the locations of local stress maximums, with the corresponding value listed inside. The local maximum tensile and compressive stresses for each figure are listed in Table 2. Absolute maximums for each case are indicated.

Maximum surface and interior stresses occurred in characteristic locations. Surface maximums occurred along the facing surfaces of the outer flow holes which face each other and along the outer surfaces of the middle ring of flow holes (see Figures 11-16). It may be noted that these stresses were located in elements adjacent to thicker core brick

TABLE 2. Maximum Stresses

Stresses tabulated are those indicated on Figures 11-16. Notation: stress/element number, stresses in MPa.

Case 1		Case 2		Case 3	
Blowdown	Reheat	Blowdown	Reheat	Blowdown	Reheat
2.8/412	-1.9/ 43	2.6/ 43	-1.1/ 27	1.9/ 60	-.83/ 43
5.2/101	-4.3/101	6.8/101	-5.3/101	4.3/101	-3.3/101
5.2/195	-4.3/185	7.9/185	-6.6/185	5.1/195	-4.3/185
5.2/194	-4.3/194	7.4/194	-6.2/194	4.7/194	-3.9/194
5.3/233*	-4.4/233*	8.1/233*	-6.8/233*	5.2/233*	-4.4/233*
5.1/262	-4.0/262	7.6/273	-6.0/273	5.0/262	-4.0/262
2.3/319	-1.7/319	3.5/319	-2.6/319	2.3/319	-1.7/319
2.1/352	-1.6/352	3.2/352	-2.3/352	2.1/352	-1.6/352
-3.2/215	2.8/189	-5.0/189	4.5/189	-3.1/215	2.8/189

*Maximum in each case.

wet sections: element numbers 60, 43 or 27, 101, 185 or 195, 194, 233, 262 or 273, 319, and 352. Interior stress maximums were located in the center of the thinner core brick wet sections. Specifically, they were found in the center of the web sections between holes of the outer flow hole ring; element numbers 189 or 215.

Some comparative observations may be made. Comparing stresses between Case 1 and Case 2 shows that the lower temperature Case 2 has greater thermal stresses. This is due to larger gas-ceramic temperature differences in Case 2, resulting in greater temperature profile curvature. In comparing stresses between Cases 3 and 1 it can be seen that the adiabatic brick perimeter had little or no effect on the maximum brick stresses.

Study of the actual MTSFF core after 1100 hours of operation reveals general confirmation of the finite element analysis. Cracking and initiation of fractures in the core bricks occurred at the locations of local surface stress maximums shown in Figures 11-16. The finite element model predicts lower stresses for the highly fractured region, Case 1, than it does for the essentially undamaged region, Case 2. This apparent reversal may be explained by a demonstrated weakening of the RFG core material at elevated temperatures [18], as shown in Figure 17. The stresstemperature states of Cases 1 and 2 are also indicated on Figure 17. Roberts [15] also supports this theory of strength decrease at elevated ceramic temperatures.

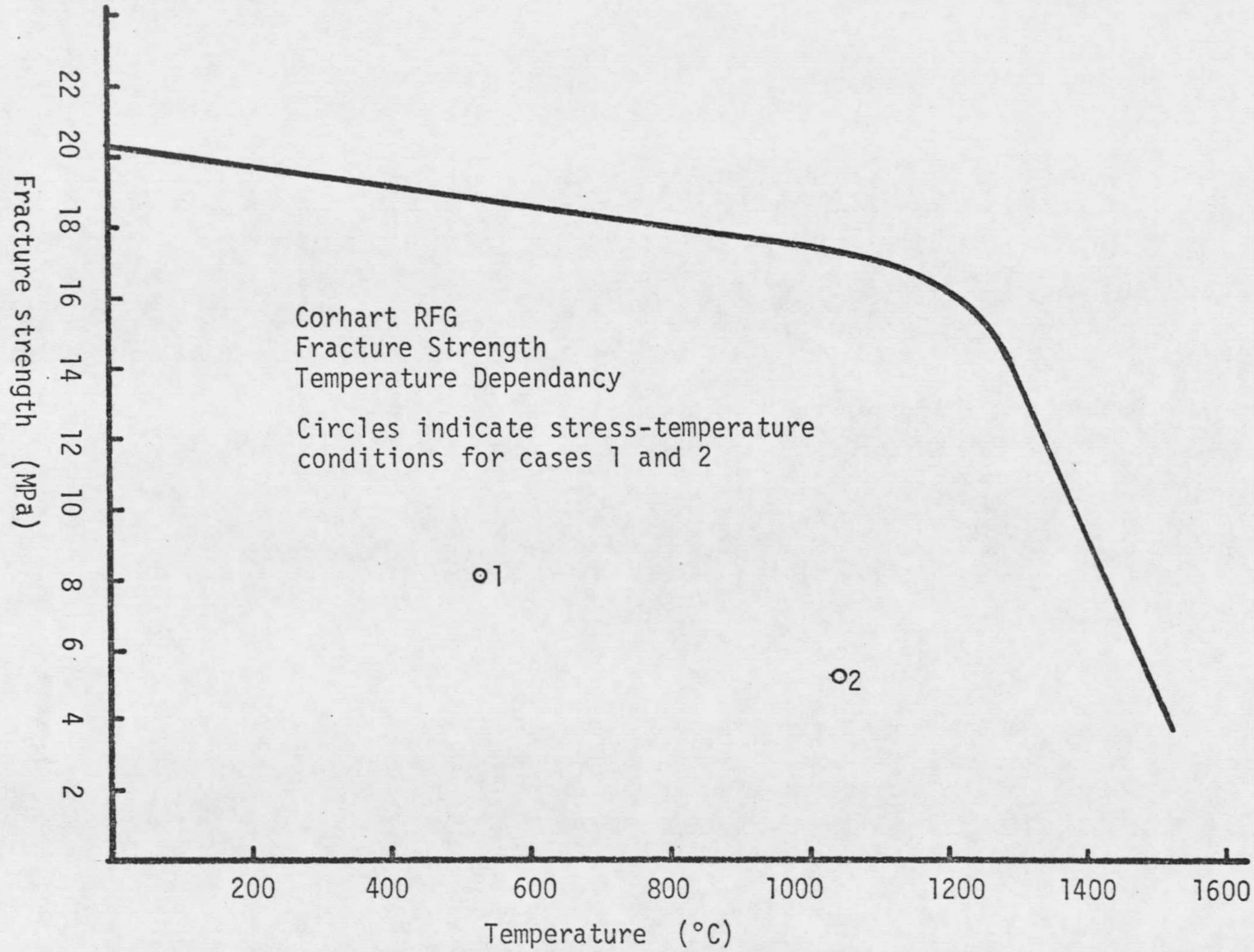

Figure 17 Corhart RFG strength-temperature correlation [18]

For comparison purposes, maximum stresses were calculated for Cases 1 and 2 using the relation presented by Upshaw [1], for axial stresses in the ceramic. For his model, the maximum tangential "hoop" stress and maximum axial stress are identical. It is the tangential stresses that must be compared to the stresses predicted by the finite element model. Only in a very long tube, longer than the 3 inch core brick height, would the axial stresses approach the values predicted by Upshaw's equation:

$$\sigma_{max} = \frac{\alpha E}{1-\nu} \frac{Qab^2}{k_c(b^2 - a^2)} \left[\frac{(b^2 - a^2)}{4b^2} + \frac{1}{2} - \frac{b^2}{(b^2 - a^2)} \ln\left(\frac{b}{a}\right)\right]$$

where: α = coefficient of thermal expansion ($°K^{-1}$),

E = modulus of elasticity (MPa),

ν = Poisson's ratio,

Q = heat flux at flow hole surface (W/m^2),

k_c = ceramic thermal conductivity (W/m-°K),

a = flow hole inner radius (m.),

b = 0.52504 S, and

S = flow hole spacing (in.).

Average heat flow rates were used for the calculations. They were based on the average reheat and blowdown gas-ceramic temperature differences. The stress values, presented in Table 3, were on the average of 40 percent higher than the values predicted in this work. They do,

TABLE 3. Maximum Stress Comparison

Stresses in MPa

		Blowdown	Reheat
Case 1	Upshaw	8.7	-5.6
	Finite Element	5.3	-4.4
Case 2	Upshaw	12.5	-8.3
	Finite Element	8.1	-6.8

however, show greater stresses at the core bottom, as did the finite element model.

CHAPTER V

CONCLUSIONS

1. The Finite Element method reasonably predicts the location of maximum stresses in a hexagonal core brick.
2. The major stresses are circumferential stresses, located at the flow hole surfaces.
3. The adiabatic boundary on Case 3 caused no significant change in stress levels from those in Case 1.

CHAPTER VI

RECOMMENDATIONS

There are two areas of possible further work in this topic. These are the result of two difficulties, one with the computer codes and one with the core brick geometry. The computer code difficulty was in duplicating actual flow conditions. It was necessary to hold gas temperatures constant throughout each cycle, unlike actual conditions, because the computer code required it. This caused initial heat transfer rates to be inaccurately high, with a similar increase in calculated stresses. The difficulty with the core brick geometry is in the large thermal mass at the brick perimeter. This is the principal cause of the large temperature change close to the brick perimeter, the major part of the "body" temperature profile. This is in the same part of the core brick as areas of maximum stress. Any connection of these two phenomena might be investigated. Therefore, two recommendations follow.

1. A different finite element heat transfer program, more advanced than HEATRANS, might be tried. This would enable more complete duplication of flow conditions.

2. Different methods of core brick construction should be studied. One possible configuration, reducing the occurrence of large thermal masses is shown in Figure 18.

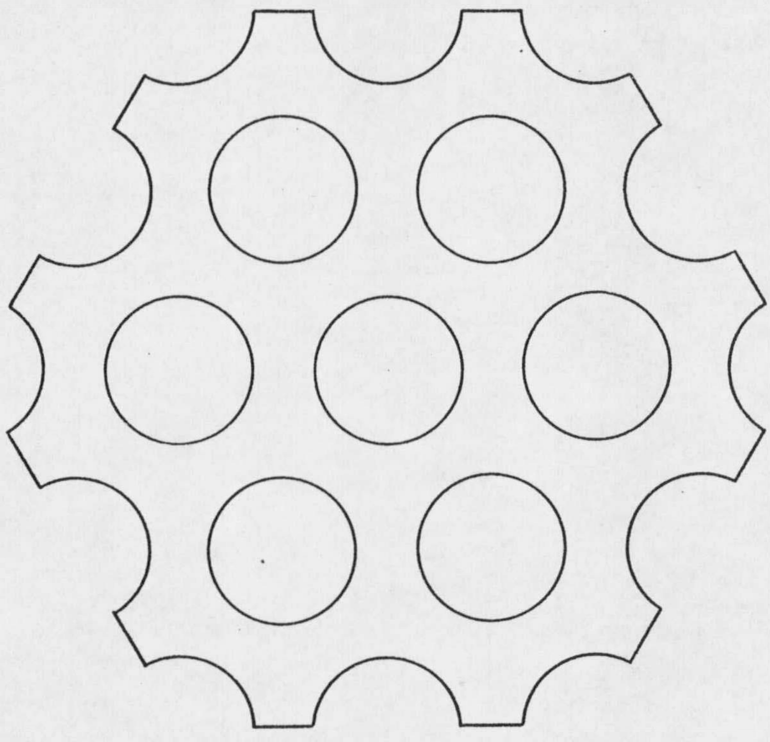

Figure 18 Suggested brick for modeling. This shape reduces large areas of thermal mass.

REFERENCES

LIST OF REFERENCES

1. Upshaw, G. W., "A Simulation Approach to the Thermal-Hydraulic Design of Cored Ceramic Brick Regenerative Heat Exchangers," Masters of Science Thesis, Mechanical Engineering Department, Montana State University, June 1977.

2. Timoshenko, S. P., and Godier, J. N., Theory of Elasticity, McGraw-Hill, Inc., New York, 1970.

3. Heubner, K. H., The Finite Element Method for Engineers, John Wiley and Sons, New York, 1975.

4. Gallagher, R. H., Fundamentals of Finite Element Analysis, Prentice-Hall, Inc., Englewood Cliffs, New Jersey, 1975.

5. Wilson, E. L., and Nickell, R. E., "Application of the Finite Element Method to Heat Conduction Analysis," Nuclear Engineering and Design, 4:276-286, 1966.

6. Cosmic Program Abstract, TAP 1-A, Computer Software Management and Information Center, University of Georgia, Feb., 1978.

7. Cosmic Program Abstract, TAP-A-A, Computer Software Management and Information Center, University of Georgia, Feb., 1978.

8. "Nastran, Nasa Structural Analysis," Program Summary, Computer Software Management and Information Center, University of Georgia, Feb., 1978.

9. Goudreau, G. L., and Nickell, R. E., and Dunham, R. S., "Plane and Axisymmetric Finite Element Analysis of Locally Orthotropic Elastic Solids and Orthotropic Shells," Report Number 67-15,

Structural Engineering Laboratory, University of California, Berkeley, August, 1967.

10. Herrick, G. C., "Analysis of Thermal Response of an Experimental Air Preheater," Masters of Science Thesis, Mechanical Engineering Department, Montana State University, July, 1978.

11. Boley, B. A., and Weiner, J. H., Theory of Thermal Stresses, John Wiley and Sons, New York, 1960.

12. Ozisik, M. N., Radiative Transfer and Interactions with Conduction and Convection, John Wiley and Sons, New York, 1973.

13. Jakob, M., Heat Transfer, Volume 1, John Wiley and Sons, New York, 1949.

14. Little, R. W., Elasticity, Prentice-Hall, Inc., Englewood Cliffs, New Jersey, 1973.

15. Roberts, C. R., Personal Communication regarding unfinished Masters of Science Thesis, Mechanical Engineering Department, Montana State University, August 1978.

16. Experimental Data Sheets, The Montana Energy and MHD Research and Development Institute, Inc., Butte, Motnana, July 1978.

17. Technical Data Sheets, Corhart Refractories Company, Inc., Louisville, Kentucky, 1976.

18. Kuszyk, J. A., and Bradt, R. C., "Microstructural Effects on Fracture and Thermal Shock of Magnesite-Chrome Refractories," Industrial Heating, 4:24-36, April 1975.

APPENDIX

APPENDIX

PROPERTIES

1. Ceramic Thermal Conductivity (W/m-°K)

   $k_c(T) = 5.355 - 0.0016\ T - 0.184 \times 10^{-6}\ T^2$

   Temperature Range: 570°K to 1800°K

   Source: Author's curve fit of experimental data [16]

2. Ceramic Thermal Expansion Coefficient (°K^{-1})

   $\alpha_T = 1.28 \times 10^{-5}$

   Temperature Range: 600°K to 1800°K

   Source: Author's curve fit of experimental data [16]

3. Ceramic Density (Kg/m^3)

   $\rho(T) = 3300\ (1 + \alpha(T - 300))^{-3}$

   Temperature Range: -----

   Source: Temperature adjustment of manufacturer's data [17]

4. Ceramic Specific Heat (J/Kg-°K)

   $C_p(T) = 961 + 0.150T$

   Temperature Range: 500°K to 1900°K

   Source: Author's curve fit of experimental data [16]

5. Ceramic Young's Modulus (MPa)

   $E = 1.1 \times 10^5$

   Temperature Range: -----

   Source: Manufacturer's data [17]

6. Ceramic Poisson's Ratio

$\nu = 0.2$

Temperature Range: -----

Source: Manufacturer's data [17]

Harris, Rodney Carl
Thermal stress in a ceramic brick air pre-heater

DATE	ISSUED TO